1 **Mechanical characterisation of the developing cell wall layers of tension wood**
2 **fibres by Atomic Force Microscopy**

3 O. Arnould[1], M. Capron[1a], M. Ramonda[2], F. Laurans[3], T. Alméras[1], G. Pilate[3], B. Clair[1]

4

5 Running title: Mechanical properties of developing secondary wall by AFM

6 [1] LMGC, Univ. Montpellier, CNRS, Montpellier, France

7 [2] CTM, Univ. Montpellier, Montpellier, France

8 [3] INRAE, ONF, BioForA, Orléans, France

9 olivier.arnould@umontpellier.fr

10 Date of submission:

11 Number of tables: 1

12 Number of figures: (colour in print) 9

13 Supplementary data number of figures, tables or videos: 3 figures

[a] Now at: Michelin, Campus RDI, Cébazat, France

1

Highlight

New insights into the changes in mechanical properties within the cell wall of poplar tension wood fibres during maturation have been obtained using atomic force microscopy.

Abstract

Trees generate mechanical stresses at the stem and branches periphery to improve their strength and to control the orientation of their axes. This key factor in the biomechanical design of trees, named "maturation stress", occurs in wood fibres during cellular maturation when their secondary cell wall thickens. In this study, the spatial and temporal stiffening kinetics of the different cell wall layers were recorded during fibre maturation on a sample of poplar tension wood using atomic force microscopy. The thickening of the different layers was also recorded. The stiffening of the CML, S_1 and S_2-layers was initially synchronous with the thickening of the S_2 layer and continued a little after the S_2-layer reached its final thickness as the G-layer begins to develop. In contrast, the global stiffness of the G-layer, which initially increased with its thickening, was almost stable long before it reached its final maximum thickness. A limited radial gradient of stiffness was observed in the G-layer, but it decreased sharply on the lumen side, where the new sub-layers are deposited during cell wall thickening. Although very similar at the ultrastructural and biochemical levels, the stiffening kinetics of the poplar G-layer appears to be very different from that described in maturing bast fibres.

Keywords

Atomic Force Microscopy; Cell wall; G-layer; Indentation modulus; Maturation; Poplar; Stiffening; Tension wood; Thickening.

Abbreviations

AFM: Atomic force microscopy

CML: Compound Middle Lamella

CCML: Cell Corner Middle Lamella

MFA: Microfibril angle

PF-QNM: Peak-force quantitative nano-mechanics

Introduction

Wood fibres have mechanical functions in the living tree. Mature wood fibres give the tree axis sufficient stiffness and strength to withstand its own weight and additional loads such as wind or fruits (Niklas, 1992). In addition to this "skeletal" function, wood fibres also have a "muscular" function that has two major goals. First, it allows the tree to control its posture by actively generating forces that can bend the axes (stem, branches) upwards or compensate for the effect of gravity (Alméras and Fournier, 2009; Fournier *et al.*, 2014; Moulia *et al.*, 2006; Scurfield, 1973). Second, it improves axes resistance to bending loads, such as wind, by a beneficial stress profile (i.e., tensile longitudinal stress at the periphery of the stem) (Bonser and Ennos, 1998; Alméras *et al.*, 2018). These mechanical stresses originate from physico-chemical changes of the fibre cell wall that would result in major deformation if they were not prevented by the older, stiff tissue, surrounding them. In place of strain, this leads to the development of a high mechanical stress named "maturation stress" or "growth stress" (Archer, 1986). These fibre properties progressively built up during their development.

The development of wood fibres is usually described in three phases: division taking place in the cambium, extension during which each cells reached its final size and shape, and maturation during which the secondary wall is developing. During this last maturation phase, constitutive polymers are progressively added to the wall from the cytoplasm, leading to the secondary wall thickening. The kinetics of fibre extension and cell wall thickening are well known and can be deduced from observations on transverse section using optical microscopy (Abedini *et al.*, 2015; Andrianantenaina *et al.*, 2019; Pérez-de-Lis *et al.*, 2022). However, the initial mechanical state of the deposited polymers, the evolution of their mechanical properties or their stress state during maturation are more difficult to measure and almost no data are available in the literature on these parameters. Data collection of time and space changes in the mechanical properties of the secondary wall is a first step toward a better understanding on the links between wood maturation and the building of wood quality. Here, we propose to measure these changes in the peculiar case of tension wood formation.

Tension wood is produced by angiosperms and characterised by a strong tensile stress in the fibre axis direction of the order of several tens of MPa. In tension wood, mechanical stress is known to be mainly generated within a specific gelatinous cell wall layer, named the G-layer (Côté *et al.*, 1969; Dadswell and Wardrop, 1955; Fang *et al.*, 2008; Ghislain and Clair, 2017; Onaka, 1949). Fibres containing a gelatinous layer are widespread in the plant kingdom and can be present in various organs and tissues (Gorshkova *et al.*, 2018). Depending on their cell wall composition, fibres can be

3

79   classified either as lignin-rich (i.e., wood fibres) or virtually lignin-free, such as part of tension wood

80   fibres (Ghislain *et al.*, 2019) or bast fibres found in flax, hemp, ramie, nettle, etc (Gorshkova and

81   Morvan, 2006). It is this latter category of fibres that is often named gelatinous fibre. Some authors

82   have proposed to call this gelatinous layer a tertiary cell wall but a dedicated article exposes several

83   arguments arguing that this term is not appropriate (Clair *et al.*, 2018). While poplar tension wood

84   fibres are of secondary origin, flax fibres are primary phloem fibres, or bast fibres. However, these

85   gelatinous fibres have several similarities in the biochemical composition of their cell walls with a

86   high content in crystalline cellulose oriented parallel to the fibre axis, very little or no lignin as already

87   mentioned, a matrix of non-cellulosic polysaccharides rich in pectic β-(1-4)-galactans and, to a lesser

88   extent, of type II arabinogalactan. The same is observed when comparing the transcriptome of

89   developing tension wood fibres and of flax phloem fibres, with multiple, distinct chitinases, β-

90   galactosidases, arabinogalactan proteins and lipid transfer proteins, compare for example Roach *et*

91   *al.* (2007) and Déjardin *et al.* (2004). Moreover, the thickening of the cell wall of flax fibres involves

92   considerable remodelling of the deposited layers: indeed, the newly formed layers of the secondary

93   cell wall of developing flax fibres, referred to as immature G_n-layer, have a loose structure that will

94   get more and more compact and stiff during their maturation toward a G-layer (Goudenhooft *et al.*,

95   2018; Petrova *et al.*, 2021).

96

97   The mechanisms responsible for the generation of high tensile stress during G-layer maturation are

98   still the subject of debate. Several hypothetical models have been proposed, which are reviewed in

99   Alméras and Clair (2016). Gaining knowledge on the chemical, physical and mechanical states of the

100   constitutive materials and their changes during cell wall maturation have proven particularly useful

101   in distinguishing between these models. For example, it has been observed that the G-layer contains

102   mesopores of several nanometres (Chang *et al.*, 2009; Clair *et al.*, 2008), and that these pores swell

103   during maturation (Chang *et al.*, 2015). It has also been shown that crystalline microfibrils are

104   progressively put under tension during maturation (Clair *et al.*, 2011). The synchronicity between

105   these two phenomena supports the hypothesis that pore swelling is related to the induction of tensile

106   stress in the crystalline microfibrils and thus to maturation stresses in the G-layer (Alméras and Clair,

107   2016). A crucial factor is the change in cell wall stiffness during maturation. Indeed, using mechanical

108   modelling, it has been shown that the relative kinetics of stiffening and stress induction affect the

109   resulting state of stress in the tree (Alméras *et al.*, 2005; Pot *et al.*, 2014; Thibaut *et al.*, 2001). As

110   reported by Thibaut *et al.* (2001), the tendency of the material to deform in response to physico-

111   chemical changes can result in stress of high magnitude only if the cell wall is already sufficiently

112   stiff. To the best of our knowledge, information on the stiffening kinetics of wood cell wall layers is

113   currently lacking and the only measurements available are at the tissue scale (Grozdits and Ifju, 1969;

4

114   Pot *et al.*, 2013a; 2013b).

115

116   One of the most promising and frequently used techniques today, nanoindentation, probes the

117   mechanical properties at the cell wall scale. It enables access to the mechanical properties within the

118   cell wall layers with modifications reduced to a minimum. This technique has already been used to

119   estimate the indentation modulus of mature native or thermo-mechanically modified cell walls of

120   wood fibres (Eder *et al.*, 2013), lignifying spruce tracheid secondary cell walls (Gindl *et al.*, 2002)

121   and (thick) fibre cell walls within a maturing vascular bundle of bamboo (Huang *et al.*, 2016; Wang

122   *et al.*, 2012). However, as widely recognized in the case of metallic materials, the radius of the

123   plastically affected volume around the indenter is about three times the residual indent size for an

124   isotropic material, and even more for the elastically affected one (Johnson 1987; Sudharshan Phani

125   and Oliver, 2019). This technique therefore requires a layer thickness at least three times the size of

126   the indent, which are typically in the micrometre range, to avoid measurement artefacts (Jakes *et al.*,

127   2009). As the width of the cell wall layers in the developing and maturation stages vary from almost

128   zero (cambium, beginning of the layer deposition) to a few micrometres (mature S_2 and/or G-layer),

129   interpreting the measurements obtained by nanoindentation in the presence of a gradient of properties

130   or within a thin layer is not straightforward, nor possible close to the cambium, due to boundary

131   effects. In such cases, atomic force microscopy (AFM) appears to be the best way to perform

132   mechanical measurements within each cell wall layer (Arnould and Arinero, 2015; Casdorff et al.,

133   2017; 2018; Clair *et al.*, 2003, Coste *et al.*, 2021; Nair *et al.*, 2010; Normand *et al.*, 2021). This

134   technique has already been used to investigate, for example, the development of bast fibres within a

135   flax stem (Goudenhooft *et al.*, 2018) and of the primary cell walls in the inner tissues of growing

136   maize roots (Kozlova *et al.*, 2019).

137

138   The aim of the present work was to measure changes in the indentation modulus of each cell wall

139   layer during the maturation of poplar tension wood fibres using AFM. As it was not possible to

140   monitor the maturation of a single cell over time, as a proxy, we chose to perform measurements on

141   several cells in the same row, from cambium to mature wood, that were therefore at different stages

142   of development. Using the kinetics of cell wall thickening as a basis for comparison, the stiffening of

143   the different layers of the cell wall was compared to other known phenomena such as changes in

144   mesoporosity and in crystalline cellulose strain. In addition, thanks to the nanometric spatial

145   resolution of AFM measurements, we investigated G-layer stiffening during thickening, i.e., the

146   kinetics of stiffening within the G-layer, and fluctuations in the mechanical states of a new freshly

147   deposited sub-layer. Finally, the kinetics and stiffness gradient of the poplar G-layers were compared

148   with data available in the literature on flax phloem fibres containing a gelatinous layer.

149

Materials and methods

Sample preparation

The experiments were conducted on a wood sample cut out of a young hybrid poplar tree (*Populus tremula × Populus alba*, INRA clone 717-1-B4) tilted to induce the production of tension wood. This clone was chosen as it is easy to multiply and has therefore already been used for several studies related to tension wood formation (Abedini *et al.*, 2015; Guedes *et al.*, 2017; Lafarguette *et al.*, 2004). This hybrid poplar plant was grown upright in a controlled greenhouse (located at INRAE, Orléans, France) for two months before inducing the formation of tension wood on the upper side of its stem, by tilting the plant 30° from the vertical and holding it in this position by binding the stem to a rigid stick. No up-righting process was thus allowed, which ensured the formation of tension wood on almost all the length of the stem and during the whole period. Twenty-two days after tilting, a 5-cm long stem section (estimated diameter 1 cm) was collected at the base of the stem, at around 10 cm above the ground. Small wood sub-samples, a few mm in size, were cut out of the tension wood side and fixed for 4 h in 2.5% formaldehyde and 0.1% glutaraldehyde in 0.1M McIlvaine citrate-phosphate buffer, pH 6.8, followed by 3×10 min under moderate vacuum. After thorough rinsing in McIlvain buffer, the sample was partially dehydrated in increasing series (25%, 50%, 70%) of ethanol and progressively impregnated with LR-White medium grade resin (Agar Scientific Ltd, Stansted, UK), in a series of resin and ethanol mixes containing a progressively increasing percentage of resin (20% 2h, 40% 4h, 60% 4h, 80% 24h, 100% 2+8 days). During the last pre-embedding step, in pure resin, the sample was placed under moderate vacuum for 3×10 minutes. Finally, the samples were embedded in gelatine capsules filled with pure resin and heated in an oven at 56°C for 24 h for polymerization. Semi-thin transverse sections (0.5 to 1 µm) were cut with a Histo diamond knife (Diatome Ltd, Nidau, Switzerland) installed on a Ultracut S microtome (Leica Microsystems, Vienna, Austria) to trim the block. To avoid the deformation commonly observed in G-layers as a result of their swelling, detachment and collapse after stress release (Clair *et al.*, 2005a; 2005b), at least the first 50 µm of the sample were trimmed and discarded. Finally, very thin sections (about 50 nm thick in the last step) were made at a low cutting speed (≈1 mm/s) using an Ultra AFM diamond knife (Diatome Ltd, Nidau, Switzerland) to obtain a nearly perfect flat surface. AFM measurements were carried out on the remaining block.

### *Optical measurement of the cell wall layer thickness*

After AFM experiments, semi-thin transverse sections (0.9 µm) were cut with a Histo diamond knife (Diatome Ltd, Nidau, Switzerland) installed on an Ultracut R microtome (Leica Microsystems SAS,

6

183   Nanterre, France). These sections were stained using Richardson's azur II and methylene blue

184   (Richardson *et al.*, 1960) and mounted on slides using Canada balsam. The slides were observed

185   under a light microscope (DMLP, Leica Microsystems SAS, Nanterre, France) with immersion oil

186   lenses (Fig. 1). Richardson's staining makes possible an easy detection of the presence of the G-layer

187   in wood fibres of poplar, proof of the occurrence of tension wood. Conversely, the absence of G-layer

188   indicates that no tension wood was present, as can be observed on the wood formed before tilting (on

189   the right side in Fig.1). This has been confirmed by the absence of an additional G-layer in the

190   following AFM observations.

191
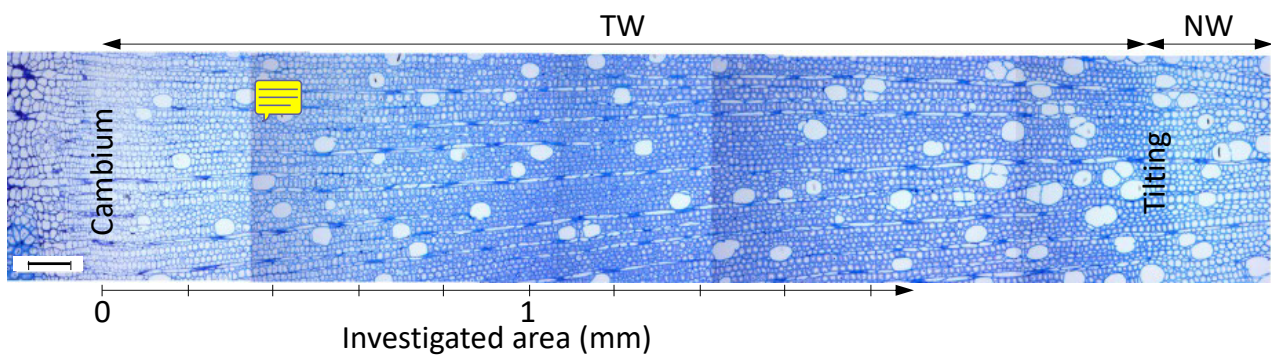
193   *Fig. 1. Optical image of the transverse section of the wood sample (Richardson's staining) with the*

194   *tension wood (TW) area between the cambium and the normal wood (NW) produced before the tree*

195   *was tilted. The reference distance from the cambium was measured approximately in the middle of*

196   *the cambial zone. Scale bar = 0.1 mm.*

197

198   Phase contrast microscopy is preferable to bright field microscopy when observing the cell wall layer

199   with high magnification (×600) as the specimen is thin, so the colour contrast is reduced (Abedini *et*

200   *al.*, 2015). Several images were acquired using a light microscope with a digital camera (DFC320,

201   Leica Microsystems SAS, Nanterre, France) from the cambium to a distance of about 2 mm from it

202   on the xylem side (i.e., with fully matured fibres), with a sufficient overlap to allow the image to be

203   repositioned to accurately measure the distance of each cell from the cambium. The mean thickness

204   of the S_2 and G layers was measured all along two radial rows using Matlab software (MathWorks

205   Inc., Natick, Massachusetts, USA) according to the method of Yoshinaga *et al.* (2012). External

206   contours of the lumen, S_2 and G layers were plotted by hand from images and their average thickness

207   was calculated as (Abedini *et al.*, 2015):

208    $$Th_G = \frac{2A_G}{P_G + P_{lumen}},$$ (1)

209 $$Th_{S2} = \frac{2A_{S2}}{P_{S2}+P_G},$$ (2)

210 where A_G and P_G are the area and the external perimeter of G-layer, respectively, A_{S2} and P_{S2} are the

211 area and the external perimeter of the S_2 layer, respectively, and P_{lumen} is the lumen perimeter. The

212 data presented in the present article show the thickness of each layer normalized by the mean cell

213 diameter, D, which was evaluated as $D = \frac{P_{S2}}{\pi}$. The advantage of working with relative thickness is

214 that it allows the effect of the fibre ends on the cell wall thickness to be corrected (Okumura *et al.*,

215 1977; Abedini *et al.*, 2015).

216

217 *AFM PF-QNM measurements*

218 Mechanical characterisation was performed with a Multimode 8 AFM (Bruker, Palaiseau, France) in

219 PF-QNM imaging mode with a RTESPA-525-30 (Bruker) probe. The spring constant of the probe

220 was calibrated by Bruker using a laser Doppler vibrometer with a value of 158 N/m. The initial tip

221 radius, 33 nm (controlled by Bruker), was checked after adjusting the cantilever deflection sensitivity

222 on sapphire and corrected to 40 nm to obtain the right range of indentation modulus on the centre of

223 DuPont™ K48 Kevlar® fibres (~20 GPa) embedded in Epofix (Struers SAS, Champigny sur Marne,

224 France) epoxy resin (~4 GPa), as described in Arnould *et al.* (2017). The value of the tip radius was

225 checked indirectly, and if necessary corrected using the above-mentioned calibration sample, by

226 ensuring that the indentation modulus and the adhesion force in the embedding resin of the wood

227 sample remained constant around the wood sample and within the lumen in the cambial area. After

228 all the measurements, the final tip radius was 1██ nm. The applied maximum load was set at 200 nN

229 for all the measurements, the vertical motion for force-distance curves was set at a frequency of 2

230 kHz, and the fast scan rate was such that the scan speed was always equal to 8 µm/s regardless of the

231 size of the image (512 × 512 pixels), with a scan axis angle of 90°.

232

233 The force-distance curves obtained were automatically adjusted by a Derjaguin-Muller-Toporov

234 (DMT) contact model (Derjaguin *et al.*, 1975) to obtain the indentation modulus using Nanoscope

235 Analysis software (Bruker, Palaiseau, France), with an assumed spherical tip, a flat sample surface,

236 and taking the measured adhesion force into account. This model is one of the simplest and is suitable

237 for vitreous polymer resin and all wood cell wall layers, considering the relatively low values of their

238 Tabor parameter (Johnson and Greenwood, 1997; Xu *et al.*, 2007). The discernible layers, i.e., layers

239 that are thick enough to avoids the measurement being influenced by edge or topography effects, are

240 the cell corner middle lamella (CCML), S_1 with the primary wall (i.e., S_1-P, as in most cases, these

241 two layers are almost impossible to distinguish), S_2 and G-layers. For each of these layers, the

242   indentation modulus distribution was obtained using Gwyddion freeware (http://gwyddion.net/), see
243   Fig. S1. This distribution can be adjusted with a Gaussian function that gives the value at the
244   maximum of the distribution (i.e., mode or most frequent value in the dataset) and the standard
245   deviation of the indentation modulus. Measurements were made on three different radial rows of
246   developing cells in the wood sample, one after the other, always starting from the cambium and
247   continuing up to a distance of about 1.7 mm away, with two overlapping sets of measurements for
248   the first row to check the stability and repeatability of the measurements. Twenty-four different
249   positions (and thus cells) were measured in the two first radial rows and 12 positions in the last row.
250   As soon as it was visible, the thickness of the S_2 and G layers was measured using the same protocol
251   as for the optical images, Eqs. (1) and (2). To complete our study, and to have a reference, we
252   measured the indentation modulus and the thickness of the cell wall layers in three normal wood cells
253   (one per radial row) that had differentiated before the tree was tilted and were therefore devoid of a
254   G-layer. All the data were assembled using Matlab software (The MathWorks Inc., Natick,
255   Massachusetts, USA).

256

257   Finally, the AFM values were checked by nanoindentation measurements on a few cells located
258   700 μm from the cambium using iNano KLA nanoindenter (Scientec, Les Ulis, France) in mapping
259   mode (NanoBlitz) on a 200×200 μm (20×20 pixels) area, with a maximum force of 0.1 mN and a
260   loading frequency of 1 Hz.

261

Results

### *Mapping the indentation modulus of developing fibres*

264   The AFM measurements provided at least a map of the sample topography and a map of the
265   indentation modulus. Examples of typical maps obtained for a cell are given in Fig. 2, at a distance
266   of 740 μm from the cambium (first radial row). The different layers of the cell wall (cell corner middle
267   lamella CCML, primary cell wall P, secondary cell wall S_1, S_2 and G-layers) are clearly identifiable
268   on the indentation modulus map due to their different elastic mechanical properties. Note that part of
269   the cell contents in the lumen are identifiable (Fig. 2b), while they are not visible in the topography
270   (Fig. 2a). The different cell wall layers are also quite easy to distinguish on the topography map
271   because of the slight change in height between each layer. The height is almost uniform within the
272   G-layer, middle lamella and embedding resin in the lumen, whereas it varies around the
273   circumference in the S_1-P and S_2-layers. These variations are the opposite in the S_1-P and S_2 (S_1-P is
274   high when S_2 is low) and these extreme values were obtained perpendicular to the cutting direction
275   (white dashed arrow in Fig. 2a). These observations are typical of a cutting effect as previously

9

276   described in Arnould and Arinero (2015). Moreover, we observed limited orthoradial variations in

277   the indentation modulus of the S_2-layer around the cells. This proves that the wood fibres are rather

278   well oriented perpendicular to the cutting direction and that there will be little (or even no) bias in the

279   interpretation of the measurements due to sample misalignment (Arnould and Arinero, 2015). The

280   distribution of the indentation modulus in the different layers in Fig. 2b is given in Fig. S1.

281

(a)   (b)

282
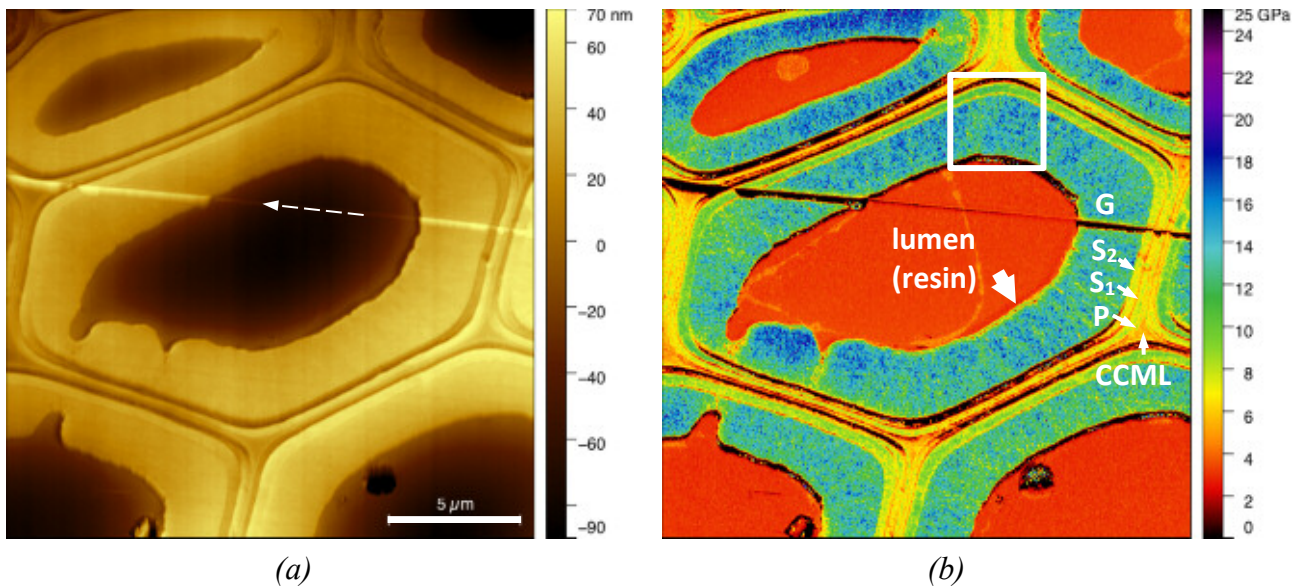
Fig. 2. PF-QNM mapping of (a) topography and (b) indentation modulus of the cross section of a tension wood fibre at 740 µm from the cambium (first radial row). The different layers are identified: P stands for primary wall and CCML for cell corner middle lamella. The lumen of the cell was filled with LR-White resin. The white dashed arrow in (a) shows the microtome cutting direction (following a scratch line due to imperfections of the diamond knife), the thick white arrow in (b) points to a thin softer sub-layer that is more visible in Fig. 4, which is an enlargement of the white upper box in (b).

289

290   Fig. 3 shows the mechanical maps of all the cells measured in the first radial row. Progressive

291   thickening of the cell wall results in the appearance of the different layers of the secondary wall: the

292   first distinguishable S_2 appears around 50 µm from the cambium (map with the green border in Fig. 3)

293   and first distinguishable G-layer around 230 µm from the cambium (map with the blue border in

294   Fig. 3). A continuous increase in the indentation modulus of the embedding resin is visible in the

295   lumen from 2.7±0.1 GPa in the cambium to 3.4±0.2 GPa at 1.7 mm. This increase was not observed

296   in the embedding resin outside the wood sample where the indentation modulus remained equal to

297   around 2.7±0.1 GPa in all the measurements. Moreover, immediate measurement of the indentation

298   modulus of the embedding resin in the lumen of cells in the cambium, taken just after the last

299   measured cell in a given row, showed a return to the initial value of 2.7±0.1 GPa.

300
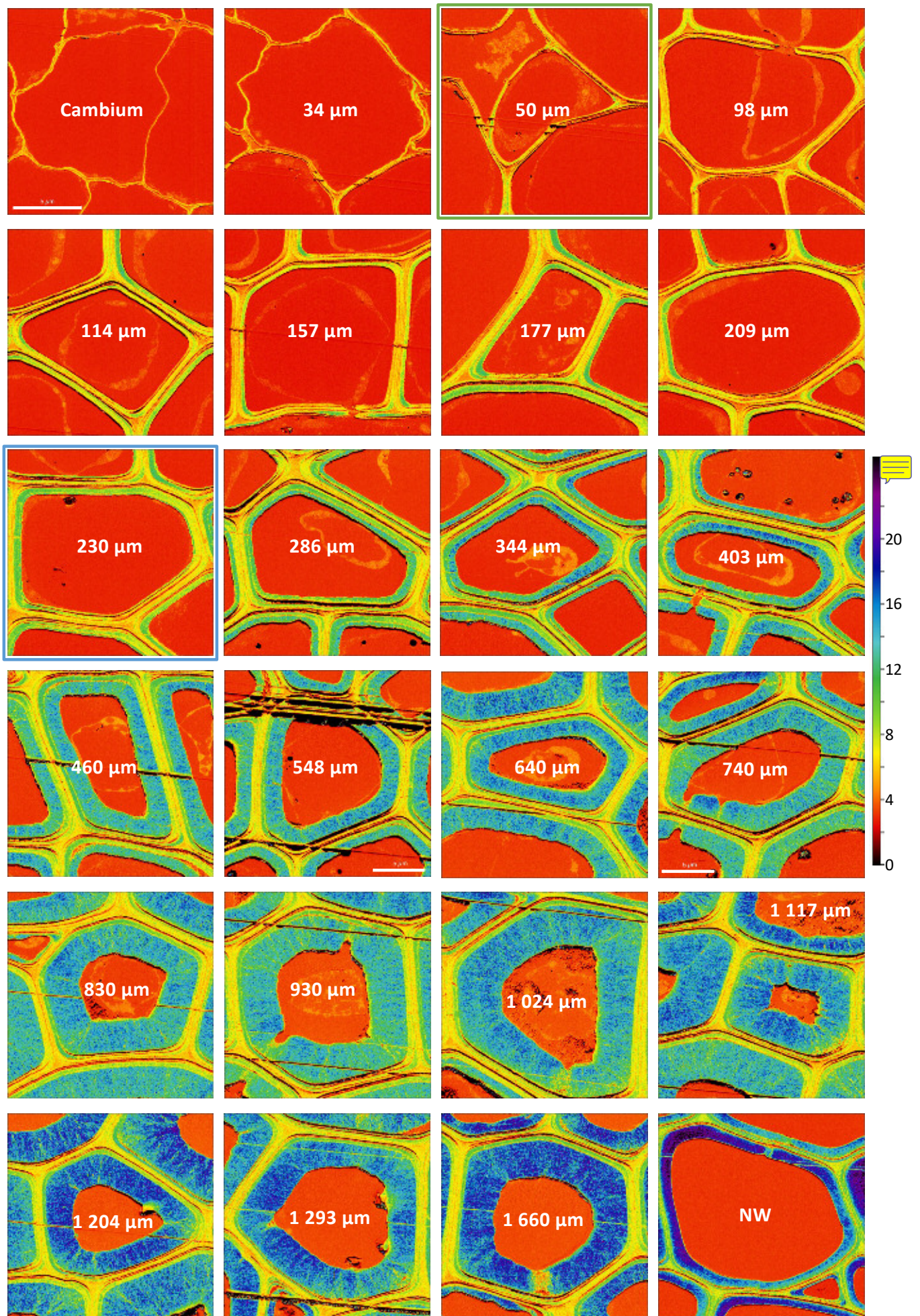
11

Fig. 3. Indentation modulus maps of the different cells measured in the first radial row. The white number in the lumen refers to the distance of the cell from the cambium, the cells are arranged in rows from left to right and from top to bottom, with the cambium always on the left. The last map on the bottom right shows a normal wood (NW) cell, here before tilting (Fig. 1). The map at 50 μm (green border) is the first map with a distinguishable S_2-layer. The map at 230 μm (blue border) is the first map with a distinguishable G-layer. Except for the maps at 548 and 740 μm, the size of the maps is same in all the images. Scale bar = 5 μm.

The indentation modulus obtained for the S_2-layer of normal wood cells 2 mm from the cambium, was around 16.9±5.5 GPa and its relative thickness was around 0.055 (see NW in Fig. 3). A more pronounced variation of the indentation modulus was observed in the S_2-layer of this cell, which is probably due to a slight misorientation of the fibre with respect surface, as already described in Arnould and Arinero (2015).

The indentation moduli of the other layers were 7.5±1.2 for the CCML and 8.2±3.1 GPa for the S_1-layer, while the indentation modulus in the embedding resin in the lumen was 2.99±0.21, a value close to that recorded in the cambium or outside of the wood sample. The indentation modulus was confirmed by nanoindentation in the embedding resin in the lumen and in the G-layer of a few cells 700 μm from the cambium with a value of 3.5±0.15 GPa and 13.5±1.3 GPa, respectively (see Table 1 for comparison).

Overall stiffening of the G-layer with increased distance from the cambium was clearly visible. A radial pattern (radial lines in the cell wall) was also visible in the G-layer, as previously reported by Sell and Zimmermann (1998). Some ring lamellae were also visible within the cell wall layers (e.g., at 548, 740, 830, 930, 1024 and 1660 μm from the cambium in Fig. 3 and in the enlargement of Fig. 2b in Fig. S2). This last structural pattern is consistent with the radial layer-by-layer thickening of the wall and has been already reported, for example, in the S_2-layer of wood fibres (Fahlén and Salmén, 2002; Casdorff *et al.*, 2018), in the G-layer of most *Salicaceae* species excepted in the poplar genera (Ghislain *et al.*, 2016), in mature (Hock, 1942) and developing G-layers of flax bast fibres (Arnould *et al.*, 2017; Goudenhooft *et al.*, 2018) and in mature hemp fibres with a G-layer (Coste *et al.*, 2020).

At a distance from the cambium equal to or greater than 448 μm, a thin and soft sub-layer was visible on the lumen side at the border of the G-layer but only on the right side of the map (as shown in

12

Fig. 2b). The fact that this sub-layer is only visible on the right side of all cells can be attributed to a cutting effect when the sample surface was prepared with the diamond knife, as the cutting direction is almost horizontal and proceeds from the right to the left (see Fig. 2a). As cutting effects are linked to the mechanical behaviour of the cell wall, this sub-layer reveals a different behaviour than the rest of the G-layer. The average indentation modulus of this sub-layer was around 8.2±2.6 GPa, close to the value of the early G-layer, at a distance of 230-286 μm from the cambium, and its thickness was around 100 nm in all cases. Fig. 4a gives a closer view of the G-layer at the top of the cell at 740 μm from the cambium (white box in Fig. 2b) and Fig. 4b is the adhesion map obtained by AFM. Although the sub-layer is not visible on the indentation map in Fig. 4a, a sub-layer with a thickness of around 100 nm and a lower adhesion force than the rest of the G-layer is also visible on the border of the lumen in Fig. 4b. We can assume that it is the same sub-layer as that observed on the right side of the indentation modulus maps. Moreover, its low adhesion force is close to that of the early G-layer (see Fig. S3).

(a)   *(b)*
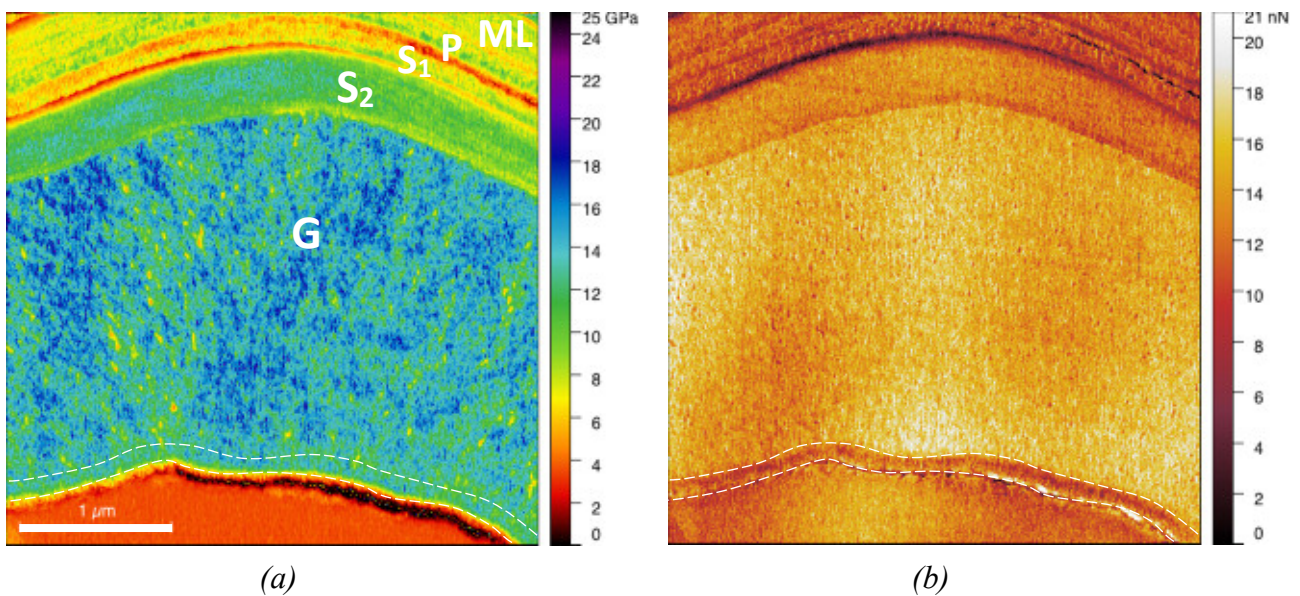
Fig. 4. a) Close-up of the indentation map of a cell taken at a distance of 740 μm from the cambium corresponding to the white box in Fig. 2b with the associated adhesion map (b) highlighted sub-G-layer with lower adhesion force close to the lumen.

To further investigate the kinetics of G-layer stiffening, we extracted six to ten radial profiles of the indentation modulus around the cell axis in the G-layer of six fibres situated at different distances from the cambium (Fig. 5). Each point in a radial profile is the average of the modulus over a width of 10 pixels. To reduce possible bias in the interpretation of the data caused by an edge effect due to cutting with the diamond knife or an effect of the area mechanically sensed by the tip (Sudharshan

Phani and Oliver, 2019), we removed the first and last 100 nm from each profile (data points in grey in Fig. 5). In contrast to the indentation modulus map in Figs. 2b and 3, where no mechanical gradient is visible in the developing G-layers, here a gradient was always visible on the last 500 nm or so on the lumen side and became less pronounced with an increase in the distance from the cambium. The gradient completely ~~disappeared~~ in the mature fibre (see Fig. 5 at 1 660 µm). It was not possible to determine whether such a gradient existed in the S_2-layer because, even if it were present, it would be hidden by the effect of the apparent microfibril angle due to the slight misalignment of the sample (Arnould and Arinero, 2015).
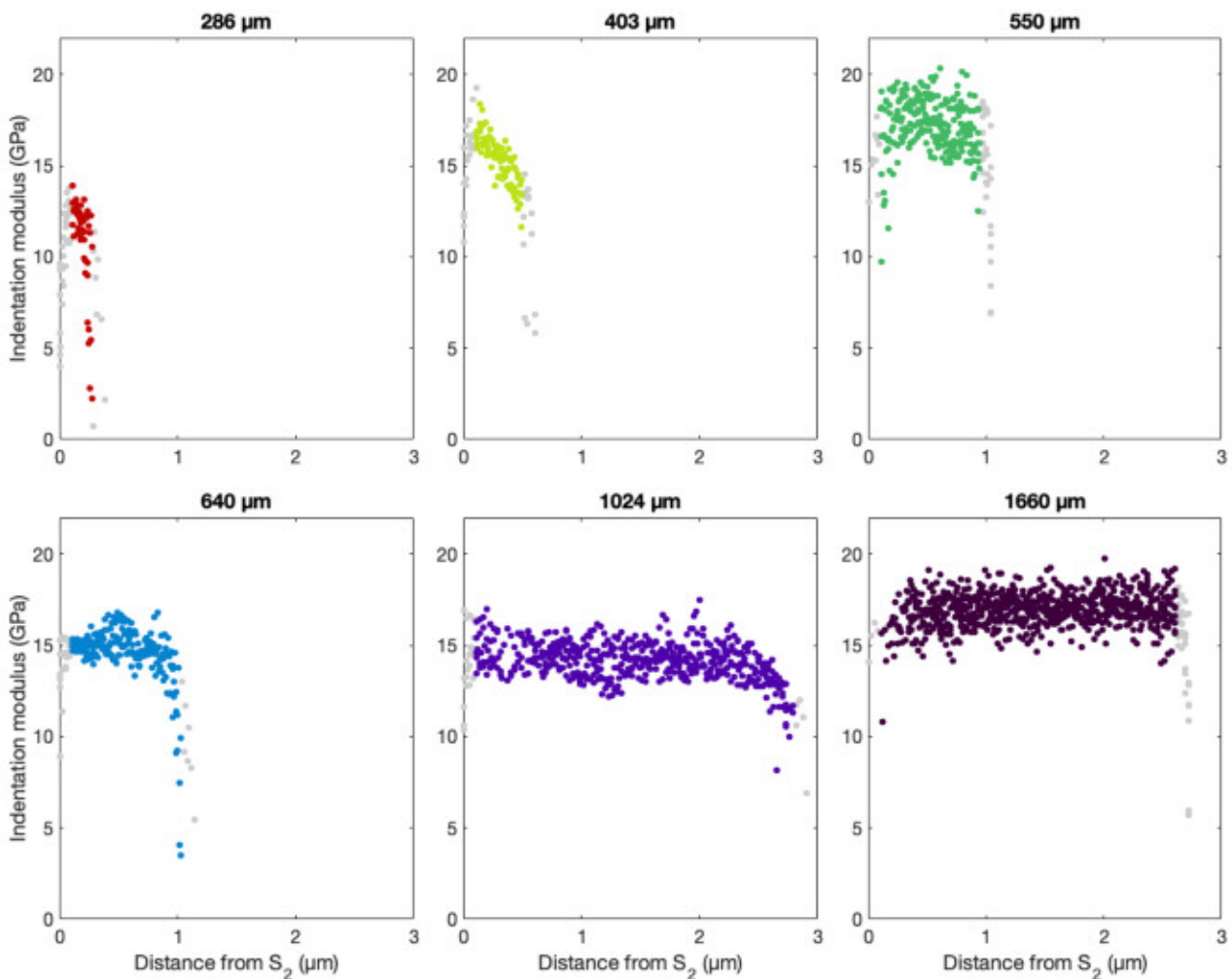
Fig. 5. Observation of the occurrence of a radial mechanical gradient during the maturation of the G-layer obtained by extracting radial profiles all around the cell axis in this layer and plotting them as a function of the distance from the S_2 layer, for fibres at six different distances from the cambium (value given at the top of each graph). The first and last 100 nm were removed from each profile (data points in grey) to avoid any bias due to possible measurement edge effects.
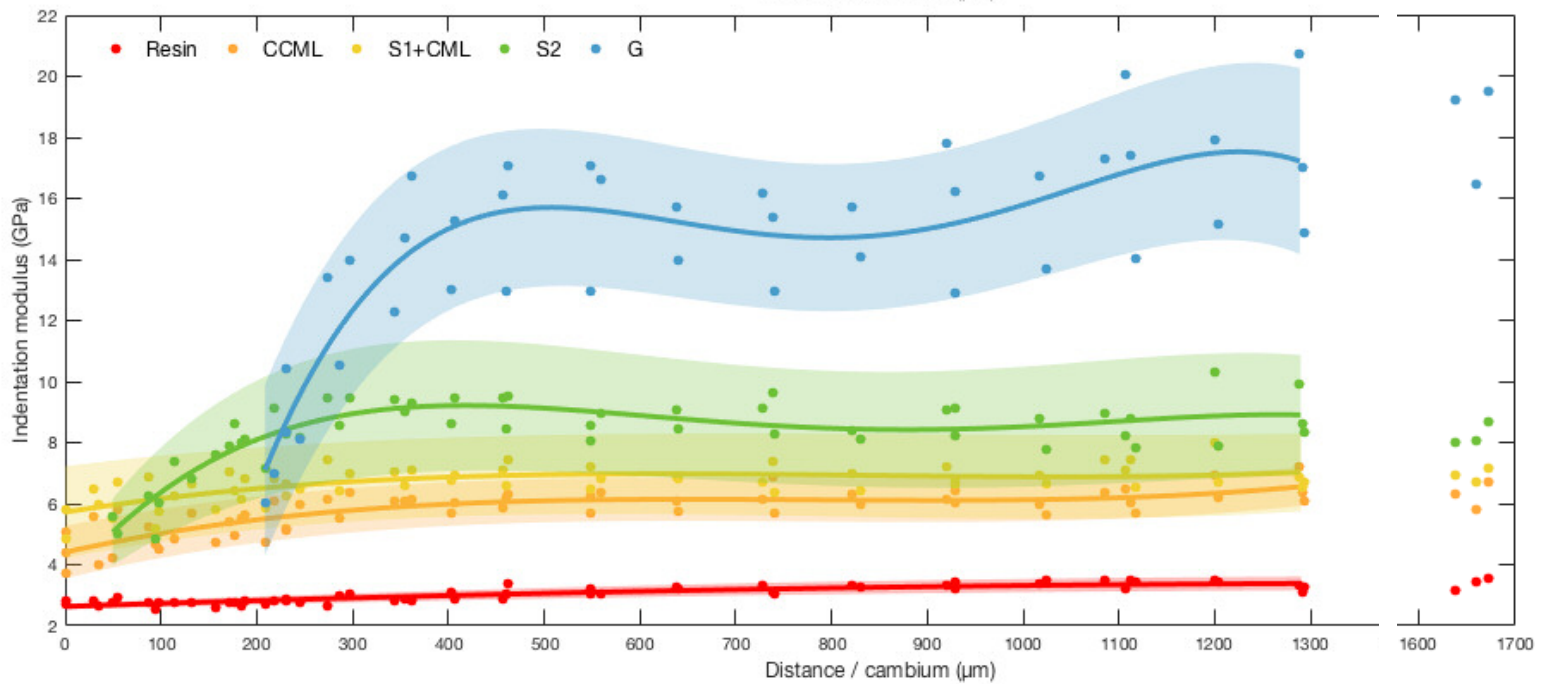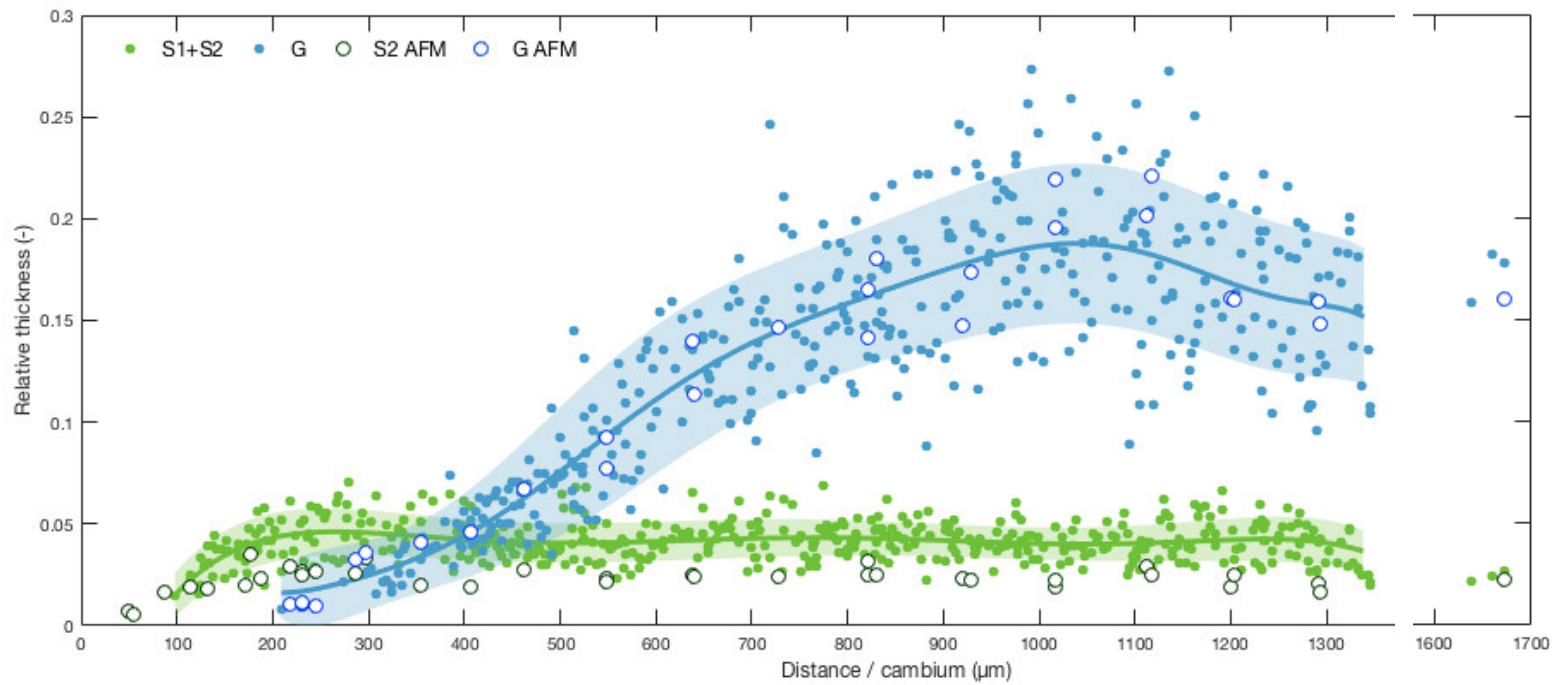
Fig. 6. Variations in the relative thickness of the cell wall layers measured by optical microscopy (coloured dots) and AFM (empty circles) (top) and mode of the indentation modulus distribution (bottom), as a function of the distance from the cambium. The solid lines and the shaded areas show the mean tendency and standard deviation adjusted on these points.

Kinetics of global cell-wall layer thickening and stiffening

All the observations made above were also made in the 2nd and 3rd radial rows. Changes in the mode of the indentation modulus distribution in each layer (e.g., see Fig. S1) are shown in Fig. 6, as a function of the distance from the cambium, together with the relative thickness of each layer. In Fig. 6, one point corresponds to one cell, whatever the radial rows, the continuous line corresponds to the mean trend adjusted on these points by a polynomial fit and the coloured ribbon to this fit shifted vertically by plus or minus the mean standard deviation on each layer of the cell wall.

In the case of the optical measurements of the thickness of the layers, it was not possible to separate the S_1 and S_2-layers, unlike for the AFM measurements. The measurements of relative thickness made by optical microscopy and AFM are consistent, but AFM enables detection of the appearance of the cell wall layer and its thickening earlier than optical microscopy. The thickness of the S_2 alone obtained by AFM is thus logically smaller than S_1+S_2 obtained by light microscopy. The relative thickness of the S_2-layer increases until around 200 μm from the cambium then decreases a little before reaching a stable value at a distance of around 500 µm from the cambium. The G-layers were first detected close to 200 µm from the cambium. The relative thickness of the G-layer increased linearly and stabilised near 1 000 µm. Thus, the relative thickness of S_2 was slightly higher before the appearance of the G-layer.

A progressive increase in the indentation modulus of both the CCML (from 4.6±0.7 to 6.1±0.7 GPa) and the S_1 layers (from 5.6±1.5 to 6.8±1.3 GPa) was observed until the end of the S_2 stiffening, at around 350 µm from the cambium. The very first S_2-layers had indentation moduli of 5.1±1.4 GPa and their stiffening and their thickening were initially synchronous. Later, when the S_2-layers reached their final thickness, their indentation modulus continued to increase and finally reached a value of 8.7±2.0 GPa. All these layers continued to stiffen when the G-layers began to thicken. In contrast, the global stiffness of the G-layer reached an almost stable plateau (at around 500 µm from the cambium) long before it attained its final maximum thickness (at around ~~1 000~~ µm from the cambium).

411 As already mentioned, as curves in Fig. 6 correspond to the mode of the indentation modulus
412 distribution (i.e., value at the maximum of the distribution or most frequent value, see Fig. S1), they
413 do not reflect the gradient observed at about 500 nm from the edge of the G-layer on the lumen side
414 due to the progressive maturation of a potentially freshly deposited sub-G-layer (Fig. 5). Furthermore,
415 as shown in Fig. 5, the thickness of the G-layer at 550 μm from the cambium is such that most of the
416 G-layer has completely stiffened, leading to the stabilised value of the indentation modulus reported
417 in Fig. 6 for this distance from the cambium.
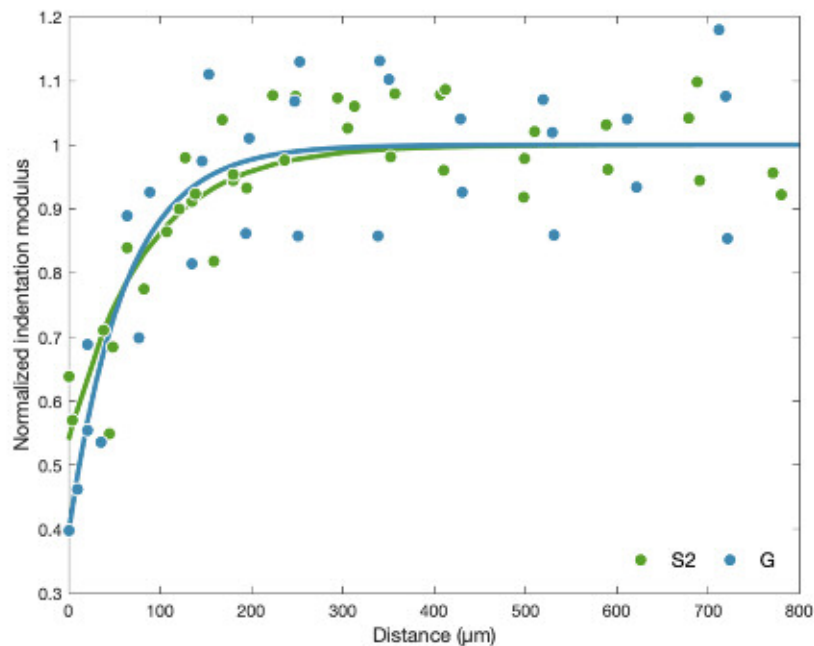
418

419 *Fig. 7. Normalized indentation modulus of the S_2 and G-layers from Fig. 6 as a function of the*
420 *distance from the cell where the layer concerned first appeared. The solid line corresponds to the*
421 *mean value.*

422

423 To compare the kinetics of the stiffening of the S_2 and G-layers, Fig. 7 shows the normalized
424 indentation modulus (i.e., the modulus from Fig. 6 divided by its mean maximum value) as a function
425 of the distance from the cell where the layer concerned first appeared (i.e., 50 μm from the cambium
426 for S_2 and 230 μm for G-layers, Fig. 3). This figure shows that the kinetics of the two layers are quite
427 similar, i.e., it took a distance of around 250 μm to globally reach their mature modulus. However, it
428 appears to be faster for the G-layer as the change in modulus from the first deposited layer to the final
429 mature one is larger.

430

Discussion

Our main results revealed: i) initial synchronous stiffening of the CML, S_1 and S_2-layers with the thickening of the S_2-layers, which continues a little after the S_2-layer has reached its final thickness while the G-layer starts to develop; ii) initial global stiffening of the G-layer synchronous with its thickening but stable global stiffness reached long before its final maximum thickness; iii) a stiffness gradient over about 500 nm on the lumen side in the developing G-layer with a softer sub-layer at the lumen edge about 100 nm in thickness.

Potential effects of sample preparation on the measurements

The different steps of sample preparation protocol made it impossible to keep the sample in its native *in planta* green state: we thus cannot rule out the possibility that modifications of the different layers of the cell wall during the ethanol exchange and resin embedding had some impacts on its mechanical properties but, for the reasons detailed below, we believe that we achieved a good compromise. Indeed, this preparation was necessary to ensure reliable mechanical measurements at small scale by AFM. Since all the measurements had to be comparable, this treatment minimised artifacts caused by roughness of the sample surface (Peaucelle, 2014). Indeed, mechanical measurements based on indentation require samples with a surface that is as flat as possible, compared to the radius of the AFM tip, to enable the use of reliable and simple contact mechanics models. These models are needed to extract the indentation modulus from the contact stiffness (Arnould and Arinero, 2015) or from the force-distance curves (Hermanowicz *et al.*, 2014). In addition, the AFM tip is very brittle and surface roughness has to be as low as possible to reduce the risk of tip wear or breakage: this is especially important in the present study where we had to perform many measurements using the same probe to limit measurement bias or drift. Moreover, AFM measurements at such a small scale are only sensitive to the very near sample surface. Damage during preparation of the sample surface should therefore be reduced to the strict minimum. In addition, as we expected to find evidence for the existence of a mechanical gradient during the thickening of the cell wall layers, we had to begin taking measurements as close as possible to the cambium, where the cell wall is very thin and soft. This is only possible when the sample has been previously embedded to avoid, or at least reduce, deformation and damage during cutting and measurements. In addition, cell wall thickening progresses from the lumen side of the cell wall and, without embedding, measurements made close to the lumen would be highly modified due to border effects (Jakes *et al.*, 2008; Jakes *et al.*, 2009) unless the lumen is filled with a sufficiently stiff substance such as resin. Finally, these embedding steps reduce cell wall layer deformation during the cutting process and avoid swelling, detachment and collapse of the G-layer commonly observed after stress release (Clair *et al.*, 2005a; 2005b).

465

Other studies have shown that LR-White embedding resin has little impact on the mechanical properties of the cell wall due to very limited penetration into the cell wall of normal wood (Coste *et al.*, 2021) and *a priori* in the G-layers of tension wood (Arnould and Arinero, 2015) and of other similar fibre cell walls such as in flax (Arnould *et al*, 2017) and hemp (Coste *et al.*, 2020). What is more, the use of ethanol is expected to cause only slight deformation of the wall. For example, Chang *et al.* (2012) showed that ethanol dehydration produced longitudinal macroscopic shrinkage of only 0.2% and volumetric swelling of only 0.5%. It is possible to avoid ethanol dehydration by drying the sample at moderate temperature just before embedding (Konnerth *et al.*, 2008). However, in the present biomechanical context with the G-layer, such a drying step would lead to very significant changes in the cell wall ultrastructure, such as mesoporosity collapse (Clair *et al.*, 2008).

The main impact of sample preparation on the mechanical properties of the cell wall is in fact its potential effects on the moisture content of the different layers. Indeed, sample preparation probably modified moisture content from a green state to close to an air-dry state. The effect of moisture content on the mechanical properties of the different cell wall layers has already been measured by nanoindentation in the cell corner middle lamella and the S_2-layer of different woody species using samples that were embedded (Wagner *et al.*, 2015) or not (Bertinetti *et al.*, 2015; Meng *et al.*, 2015). These studies revealed a similar trend with a reduction of the indentation modulus from one third to one half for the S_2-layer and at least one half for CCML, between an air-dry and saturated state. A more recent study (Coste *et al.*, 2020), using AFM PF-QNM in similar conditions to those used in our study, focused on the effect of the moisture content on the mechanical properties of hemp sclerenchyma fibres (containing a thick G-layer with similar characteristics to those of the tension wood G-layer) and xylem fibres. In their study, AFM measurements of all the cell wall layers revealed no major differences between layers, with a reduction of the indentation modulus of about one half when the relative humidity varied from 13% to 83%. If we extrapolate these variations to our study, the indentation modulus values reported here are overestimated compared to the values *in planta* but the relative differences observed between layers, or within a layer (gradient), are most probably comparable to what happens in the tree.

Indentation modulus and its variations in the different layers of the cell wall

We observed an increase in the indentation modulus of the embedding resin in the lumen, with increased distance from the cambium, but it goes back to values measured in the cambial zone in the normal wood (before tilting) cells lumen. The origin of this increase during fibre maturation is not

19

499   yet understood but is unlikely to be due to wear of the AFM tip as demonstrated by the repeatability

500   of the measurements in the cambial cells performed after measurements of each row, which were also

501   identical to those obtained at the end of all measurements in the lumen of the normal wood cells or

502   in the resin outside the sample. Stiffening thus appears to be associated with the change in the contents

503   of the lumen with the maturation of the fibres (as shown in Fig. 3). In cambial cells, the plasma

504   membrane and cytoplasm are bound to the inner part of the cell wall. Cambial cells are highly

505   vacuolated, and the large vacuole pushes the cell organelles outwards. There is therefore little material

506   inside the lumen (vacuole contents), which may explain why the indentation modulus measured in

507   the resin in the centre of cambial cells is close to that measured in normal wood cells that have lost

508   all their cell contents. Finally, Table 1 shows that our LR-White indentation modulus values were the

509   lowest compared to other authors' data, but are confirmed by nanoindentation. This is probably due

510   to differences in the calibration procedure between laboratories or to the variability of the resin itself,

511   as different grades (soft, medium, and hard) of this resin are available.

512

513   The values of the indentation modulus in the different layers and the embedding resin are consistent

514   with the (rather scattered) AFM data or nanoindentation measurements of wood cell walls available

515   in the literature (Arnould and Arinero, 2015; Clair *et al.*, 2003; Coste *et al.*, 2021; Eder *et al.*, 2013;

516   Liang *et al.*, 2020; Normand *et al.*, 2021), although in the low range compared literature data on the

517   G-layer of poplar or tension wood (see Table 1). These low values can be partly explained by the

518   young age of the tree used in our study (less than 3-month old). Indeed, the juvenile wood is known

519   for its high microfibril angle (MFA) in the S_2-layer and its low cellulose content (Luo *et al.*, 2021).

520   These low indentation modulus values may also result from the fact that the cell used as an example

521   in Fig. 2 was not fully mature. The values of the indentation modulus in the G-layer of a mature cell

522   increased to around 18.3±3.1 GPa on average (see Fig. 6), a value in the same range of the ones cited

523   in the literature (Table 1).

524

525   The low value obtained for the mature S_2-layer in the tension wood area compared to the value in

526   normal wood can be explained by a marked difference in MFA between the S_2-layers of normal wood

527   (with a low MFA and therefore a high indentation modulus) and the S_2-layers of tension wood (with

528   a high MFA and therefore a small indentation modulus, Eder *et al.*, 2013; Jäger *et al.*, 2011). To

529   explain this difference (equal to a factor of about 2) between the indentation moduli, we can roughly

530   estimate from published data that the MFA is around 5-10° in normal wood whereas it is 30-40° in

531   the S_2 of tension wood (Arnould and Arinero, 2015; Jäger *et al.*, 2011). This is also in agreement with

532   the value of MFA reported for the S_2-layer in tension wood for poplar by Goswami *et al.* (2008).

533   Likewise, the order of magnitude of the values of indentation modulus obtained for the different

534   layers of normal wood is in agreement with other literature data (Table 1).

535   *Table 1. Comparison of the value of the indentation modulus (in GPa) in the different layers of mature*

536   *wood fibres in our study and in the literature.*

Reference	LR-White resin (lumen)	ML (CC)	S_1	S_2	G
This study, developing tension wood (740 µm, Figs. 2 and S1)	3.10±0.29	5.4±1.0	6.5±1.4	8.3±2.2	13.0±3.1
This study, mature tension wood (1660 µm, Fig. 3)	3.35±0.27	5.9±1.0	6.7±1.2	8.2±2.6	16.5±3.3
This study, mature normal wood (NW, Fig. 3)	2.99±0.21	7.5±1.2	8.2±3.1	16.9±5.5	n.a.
Normand *et al.* (2021) (poplar)	3.9±1.8	9.9±1.2	11.3±0.3	16.4±0.4	16.8±0.5
Clair *et al.* (2003) (oak, no embedding)	n.a.	5-7	8-9	9-10	10-12
Arnould and Arinero (2015) (chestnut)	3.5±1.5	6±0.5	n.a.	13±0.5	15±1.5
Liang *et al.* (2020) (poplar, no embedding)	n.a.	n.a.	6.89-10.48	10.57-14.61	11.13-18.5
Coste *et al.* (2021) (poplar)	4.5±0.9	10.7±2	16.0±3.8	18.2±3.5	n.a.

537

Kinetics of global thickening and stiffening of the cell-wall layers

539   The CCML, S1 and S_2-layers continued to stiffen while G-layer was developing (Fig. 6). This is in

540   agreement with the fact that the lignification of S_1, S_2-layers and CCML occurs during the formation

541   of the G-layer (Yoshinaga *et al.*, 2012). This lignification after the G-layer starts to thicken may be

542   explained by the presence of additional matrix material that has been transported through the existing

543   wall. Alternatively, some precursors may already be present and are used in biochemical reactions

544   that continue during the deposition of the G-layer. The effect of lignification on the mechanical

545   properties of the cell wall is not yet well understood, with different studies sometimes reporting

546   conflicting results, but recent studies tend to confirm the hypothesis that lignification mainly affects

547   the shear modulus and the strength of the matrix (Özparpucu *et al.*, 2017; 2019), with higher content

548   leading to a higher modulus and greater strength. The indentation modulus is sensitive to the

549   longitudinal modulus but also to the transverse and shear moduli (Jäger *et al.*, 2011), which are mainly

550   influenced by the cell wall matrix. Therefore, when lignification modifies the cell wall matrix

551   properties, this results in a ~~significative~~ change in the indentation modulus, as already shown by

552   nanoindentation (Gindl *et al.*, 2002). Finally, Fig. 7 shows that the stiffening kinetics appear similar

553   although faster in the G-layer than in the S_2-layers suggesting that the physical and chemical changes

554   or reactions at work during cell wall maturation are faster in the G-layer (e.g., microfibrils aggregation

555   or gelatinous matrix swelling (Alméras and Clair, 2016)) than in the S_2-layer (e.g., lignification).

556

557   The fact that the relative thickness of the S_2-layer decreases slightly when the G-layer is starting to

558   develop has already been observed. For example, Abedini *et al.* (2015) reported that this is a common

559   trend throughout the growing season in both normal and tension wood of poplar trees. Moreover,

560   the changes and mature value of the relative thickness of the G and S_2 layers in Abedini *et al.* (2015),

561   Chang *et al.* (2015) and Clair *et al.* (2011) are similar to our measurements. We therefore assume that

562   we can use the relative thickening of the different wall layer as a common spatial reference to link

563   different studies. If we combine our results with those of previous studies, the G-layer appears to

564   synchronously stabilise its thickness, whole indentation modulus (i.e., no more radial gradient), meso-

565   pore size (Chang *et al.*, 2015) and cellulose tensile strain (Clair *et al.*, 2011) at the end of the

566   maturation. These observations suggest that the different changes involved in the maturation process

567   of the G-layer start, evolve and end at approximately the same fibre development stage. These

568   physico-chemical observations now need to be coupled with biochemical analyses to better

569   understand the mechanisms involved in G-layer maturation, and possibly to establish relationships

570   between matrix stiffening, bridging between microfibrils and wall compaction (Alméras and Clair,

571   2016; Gorshkova *et al.*, 2015; Mellerowicz and Gorshkova, 2012).

572

573   According to the radial profiles of the indentation modulus (Fig. 5), a smooth mechanical gradient

574   occurs in immature G-layer on less than 0.5 μm on the lumen side with a small sublayer of about

575   100 nm. This sublayer appears to be as dense as the mature part of the layer and could be either a

576   freshly deposited immature G-layer or part of the periplasmic area still bound to the layer. Indeed,

577   periplasmic area, located between the inner part of the G-layer and the plasma membrane, is the scene

578   of intense biochemical processes, see Fig. 2 in Pilate *et al.* (2004), Fig. 5 in Guedes *et al.* (2017) or

579   Fig. 7 in Decou *et al.* (2020). In contrast, flax bast fibres exhibit a strong mechanical gradient with a

580   thick immature, loose and soft G-layer, called G_n (Gorshkova and Morvan, 2006; Gorshkova *et al.*,

581   2010). Evidence for the presence of this thick G_n-layer has also been provided in flax xylem tension

582   wood fibres (Petrova *et al.*, 2021). Interestingly, the indentation modulus is similar, or even a little

583   bit higher, in flax G-layers than in mature poplar G-layers, while the average indentation modulus is

584   in the same range in flax G_n-layers, in immature poplar G-layers in fibres close to the cambium and

585   in inner sub-layers observed in more developed G-fibres.

586

587

Comparison with flax G-layer

(a)

(b)

(c)

589
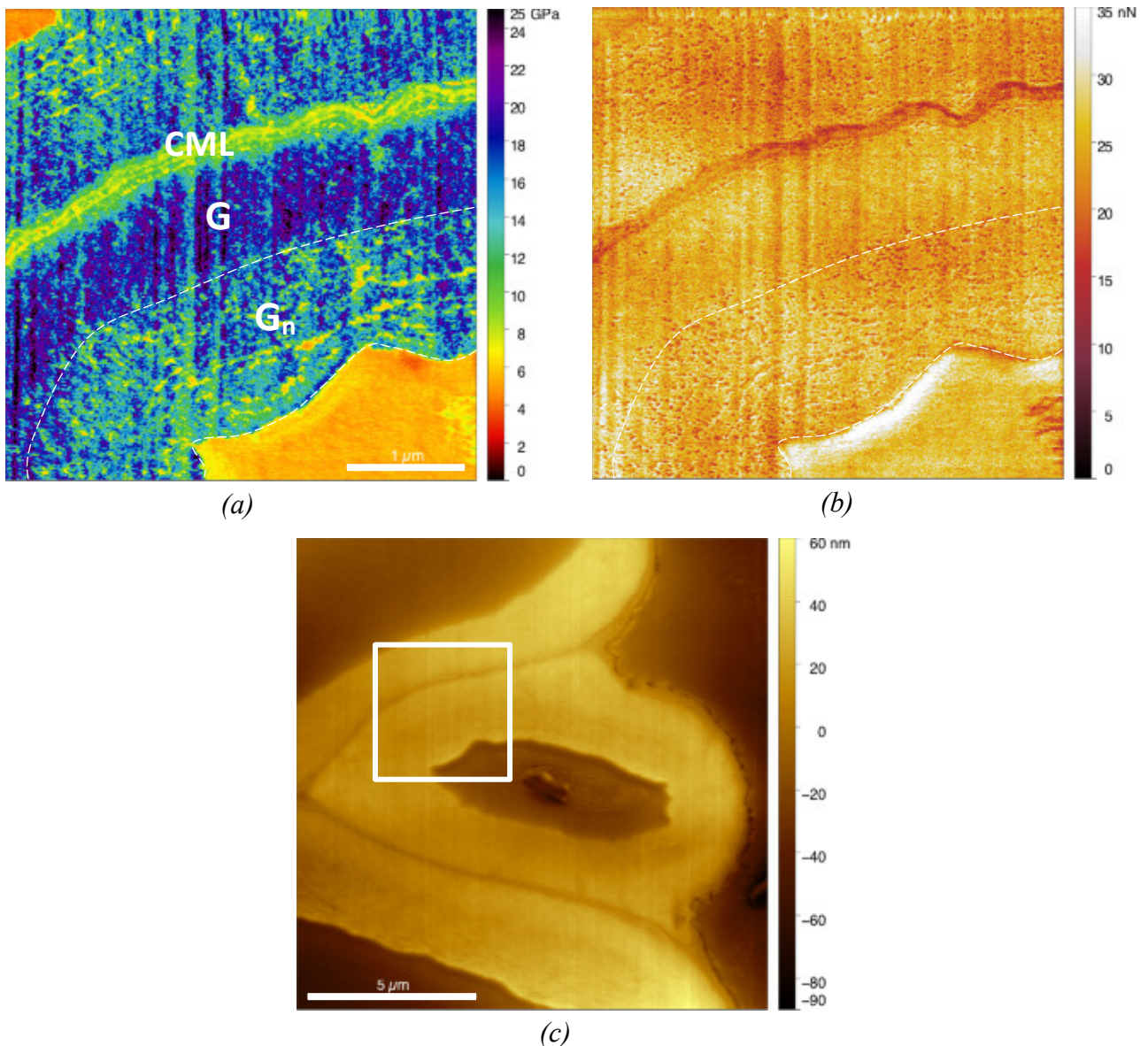
Fig. 8. Comparison of the G and G$_n$-layers in developing flax bast fibre (60 days, half height of the stem) adapted from Arnould et al. (2017): a) indentation modulus map and b) adhesion map corresponding to the white box in the topography image (c).

593

594 In a typical developing flax fibre, both indentation modulus (Arnould *et al.*, 2017; Goudenhooft *et al.*, 2018) and adhesion force exhibit a sharp transition between G and G$_n$-layers as shown in Fig. 8. However, the sublayers observed as lamellae in the G$_n$ have indentation modulus and adhesion force similar to those measured in the G-layer. These lamellae are separated by bands whose indentation modulus is close to that of the resin, but with a lower adhesion force. This lamellar arrangement is not observed in poplar, even though ring lamellae structure of this type is sometimes discernible in the mature part of the G-layer (*e.g.*, see cells at a distance of 548, 740, 830, 930, 1 024 and 1 660 µm

601 from the cambium in Figs. 3 and S2). The most significant structure in the poplar G-layer appears as
602 radial bands (*e.g.*, see tension wood fibres at a distance of more than 740 μm in Fig. 3). This pattern
603 may reflect biological organisation, but we cannot exclude a possible consequence of a slight
604 shrinkage of the G-layer during dehydration with ethanol (Fang *et al.*, 2007).

605

606 Note that it is not possible to compare the absolute value of adhesion forces obtained in the present
607 study (Fig. 4b) with the values obtained in Arnould *et al.* (2017) (in Fig. 8b) as this force depends to
608 a great extent on the shape of the tip and on the surface roughness of the material, which were not the
609 same (see for example the difference in adhesion forces of the embedding resin in the lumen in the
610 two studies, even though the same resin was used).

611
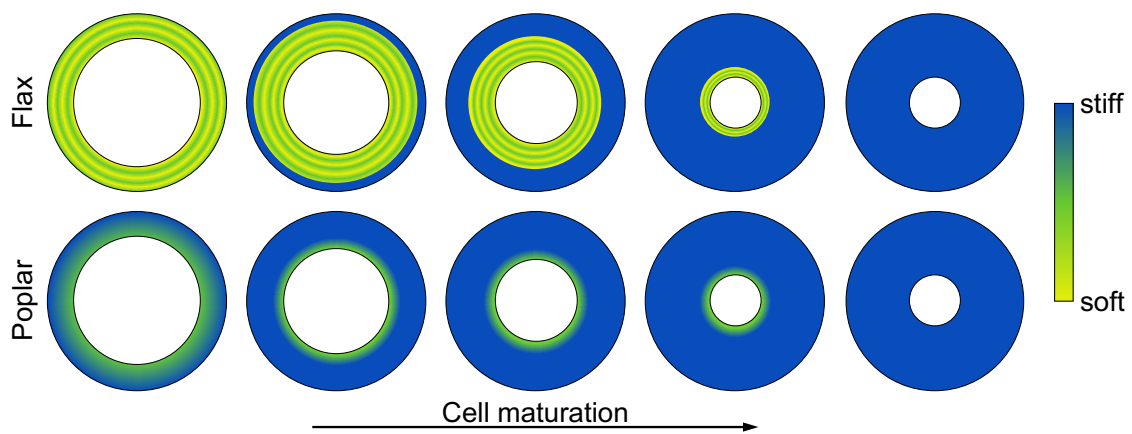
612

613 *Fig. 9. Comparative scheme of the maturation (thickening and stiffening) of the G-layer of flax and*
614 *poplar.*

615

616 Although the G-layer of tension wood and the G-layer of flax are biochemically, ultrastructurally and
617 mechanically similar (Coste *et al.*, 2020; Guedes *et al.*, 2017; Gorshkova and Morvan, 2006;
618 Gorshkova *et al.*, 2018; Petrova *et al.*, 2021), they clearly differ in the kinetic of their development
619 and maturation, as summarised in Fig. 9. Indeed, in flax, a thick and loose multilayered G_n-layer
620 stiffens and densifies abruptly, whereas, in poplar, it is a thin and dense immature layer that stiffens
621 gradually. Further complementary analyses including immunochemistry need to be done to clarify
622 the origin of these differences.

623

Conclusion

625 The use of AFM makes possible to measure simultaneously the stiffening and thickening kinetics of
626 different cell wall layers: this provides novel and precious insight into the kinetics of the maturation
627 of any kinds of wood fibre. In this study, we applied this technique ~~onto~~ poplar tension wood fibres

628 containing a G-layer: this revealed that the G-layer reaches its near final stiffness long before its final
629 thickness. In addition, we ~~evidenced~~ a radial mechanical gradient localised at the lumen periphery
630 that remains throughout the thickening and ~~disappear~~ very late in mature G-layers. This contrasts
631 with the maturation kinetics of the other cell wall layers, where thickening and stiffening are mostly
632 synchronous. Finally, although the G-layer in poplar tension wood fibres and in flax phloem fibres
633 are biochemically, ultrastructurally and mechanically similar, it is clear ~~here~~ that they differ in the
634 kinetic of their development and maturation.

635

636 The data collected in this study is not sufficient on its own to discriminate among the hypothetical
637 mechanisms of maturation stress generation, reviewed in Alméras and Clair (2016)~~, which are~~
638 ~~involved~~. In this last article, the authors found that four mechanisms were admissible to explain stress
639 generation in tension wood: (i) stress generation in amorphous cellulose domain in series with
640 crystalline domain in the microfibrils, (ii) active binding of microfibrils by a (still unspecified)
641 material, (iii) entrapment of material during microfibrils aggregation and cell wall compaction as
642 suggested for flax bast fibres (Goudenhooft et al., 2018) (see Fig. 8b-c too) and (iv) swelling of the
643 matrix in a connected cellulose network. In order to discriminate these different mechanisms, it is
644 necessary to estimate their respective effects on the mechanical properties of the cell wall, and to
645 estimate the resulting effect on the indentation modulus. Indentation modulus is a complex
646 combination of different elastic parameters, particularly longitudinal, transverse and shear elastic
647 properties (Jäger *et al.*, 2011), the two ~~lasts~~ are particularly sensitive to the "matrix" moduli (i.e.,
648 matrix and binding between microfibrils). Thus, the first mechanism of maturation stress generation
649 would probably have almost no effect on the cell wall mechanical properties, if not accompanied by
650 a change in the matrix mechanical properties. Active binding and cellulose aggregation may have
651 similar stiffening effect, in that it would lead to an increase in the shear and transverse elastic
652 properties of the cell wall. Matrix swelling could lead to an apparent stiffer matrix (isotropic)
653 property, but probably with lighter effect than the two previous mechanisms. So, information about
654 the change along the maturation process in the cell wall longitudinal, shear and transverse properties
655 ratio is critical. Finally, more than one mechanism could be involved together or at different ~~step~~ of
656 the maturation. For example, it is possible that the slight and homogeneous increase in the indentation
657 modulus that can be seen in Fig. 5 between 1024 μm and 1660 μm from the cambium and in Fig. 6
658 for a distance from the cambium greater than 900 μm, ~~so~~ after the stiffening process described in the
659 present study, was due to another stiffening mechanism. Further studies on the composition and
660 structure of the G-layer (including, for example, immunochemistry) definitely need to be done in
661 order to advance our knowledge.

662

Acknowledgements

Author contributions

OA participated in sample preparation, supervised and designed all the experiments and data analysis, performed some of them, and contributed to writing the original draft of the paper. MC performed some of the experiments and the data analysis, wrote the original draft of the paper. MR supervised and performed all the experiments. FL prepared the sample and contributed fruitful discussions to the data analysis. TA contributed to data analysis and to writing the original draft of the paper. GP contributed to data analysis. BC contributed to data analysis, conceptualised and supervised the whole project. All the authors reviewed and edited the paper and approved the final version.

Data availability statements

The datasets used during the current study are freely available on the open repository website Zenodo: https://doi.org/10.5281/zenodo.6487575.

References

Abedini R, Clair B, Pourtahmasi K, Laurans F, Arnould O. 2015. Cell wall thickening in developing tension wood of artificially bent poplar trees. IAWA Journal **36**, 44-57.

Andrianantenaina AN, Rathgeber CBK, Pérez-de-Lis G, Cuny H, Ruelle J. 2019. Quantifying intra-annual dynamics of carbon sequestration in the forming wood: a novel histologic approach. Annals of Forest Science **76**(3), 1-12.

Alméras T, Gril J, Yamamoto H. 2005. Modelling anisotropic maturation strains in wood in relation to fibre boundary conditions, microstructure and maturation kinetics. Holzforschung **59**, 347-353.

Alméras T, Fournier M. 2009. Biomechanical design and long-term stability of trees: Morphological and wood traits involved in the balance between weight increase and the gravitropic reaction. Journal of Theoretical Biology **256**, 370-381.

Alméras T, Clair B. 2016. Critical review on the mechanisms of maturation stress generation in trees. Journal of the Royal Society Interface **13**, 20160550.

695 **Alméras T, Jullien D, Gril J.** 2018. Modelling, evaluation and biomechanical consequences of
696 growth stress profiles inside tree stems. In: Geitmann A, Gril J, eds. Plant biomechanics: From
697 structure to function at multiple scale. Berlin: Springer, 21-48.

698 **Archer RR.** 1986. Growth stresses and strains in trees. In: Timell TE, ed. Springer Series in Wood
699 Science, Berlin Heidelberg: Springer.

700 **Arnould O, Arinero R. 2015.** Towards a better understanding of wood cell wall characterisation
701 with contact resonance atomic force microscopy. Composites: Part A **74**, 69-76.

702 **Arnould O, Siniscalco D, Bourmaud A, Le Duigou A, Baley C.** 2017. Better insight into the nano-
703 mechanical properties of flax fibre cell walls. Industrial Crops and Products **97**, 224-228.

704 **Bertinetti L, Hangen UD, Eder M, Leibner P, Fratzl P, Zlotnikov I.** 2015. Characterizing
705 moisture-dependent mechanical properties of organic materials: humidity-controlled static and
706 dynamic nanoindentation of wood cell walls. Philosophical Magazine **95**, 1992-1998.

707 **Bonser RHC, Ennos AR.** 1998. Measurement of prestrain in trees: implications for the determination
708 of safety factors. Functional Ecology **12**, 971-974.

709 **Casdorff K, Keplinger T, Burgert I.** 2017. Nano-mechanical characterization of the wood cell wall
710 by AFM studies : comparison between AC- and QI mode. Plant Methods **13**, 60.

711 **Casdorff K, Keplinger T, Rüggeberg M, Burgert I**. 2018. A close-up view of the wood cell wall
712 ultrastructure and its mechanics at different cutting angles by atomic force microscopy. Planta **247**,
713 1123-1132.

714 **Chang SS, Clair B, Ruelle J, Beauchêne J, Di Renzo F, Quignard F, Zhao GJ, Yamamoto H,**
715 **Gril J.** 2009. Mesoporosity as a new parameter in understanding of tension stress generation in trees.
716 Journal of Experimental Botany 60, 3023-3030.

717 **Chang SS, Quignard F, Di Renzo F, Clair B.** 2012. Solvent polarity and internal stresses control
718 the swelling behavior of green wood during dehydration in organic solution. BioResources **7**, 2418-
719 2430.

720 **Chang SS, Quignard F, Alméras T, Clair B.** 2015. Mesoporosity changes from cambium to mature
721 tension wood: a new step toward the understanding of maturation stress generation in trees. New
722 Phytologist **205**, 1277-1287.

723 **Clair B, Arinero R, Leveque G, Ramonda M, Thibaut B.** 2003. Imaging the mechanical properties
724 of wood cell wall layers by atomic force modulation microscopy. IAWA Journal **24**, 223-230.

725 **Clair B, Gril J, Baba K, Thibaut B, Sugiyama J.** 2005a. Precaution for the structural analysis of
726 the gelatinous layer in tension wood. IAWA Journal **26**, 189-195.

727 **Clair B, Thibaut B, Sugiyama J.** 2005b. On the detachment of gelatinous layer in tension wood
728 fibre. Journal of Wood Science **51**, 218-221.

729 **Clair B, Gril J, Di Renzo F, Yamamoto H, Quignard F.** 2008. Characterization of a gel in the cell
730 wall to elucidate the paradoxical shrinkage of tension wood. Biomacromolecules **9**, 494-498.

731 **Clair B, Alméras T, Pilate G, Jullien D, Sugiyama J, Riekel C.** 2011. Maturation stress generation
732 in poplar tension wood studied by synchrotron radiation micro-diffraction. Plant Physiology **155**,
733 562-570.

734 **Clair B, Déjardin A, Pilate G, Alméras T.** 2018. Is the G-layer a tertiary cell wall? Frontiers in
735 Plant Science **9**, 623.

736 **Coste R, Pernes M, Tetard L, Molinari M, Chabbert B.** 2020. Effect of the interplay of
737 composition and environmental humidity on the nanomechanical properties of hemp fibers. ACS
738 Sutainable Chemistry and Engineering **8**, 6381-6390.

Coste R, Soliman M, Bercu NB, Potiron S, Lasri K, Aguié-Béghin V, Tetard L, Chabbert B, Molinari M. 2021. Unveiling the impact of embedding resins on the physicochemical traits of wood cell walls with subcellular functional probing. Composites Science and Technology **201**, 108485.

Côté WA, Day AC, Timell TE. 1969. A contribution to the ultrastructure of tension wood fibers. Wood Science and Technology **3**, 257-271.

Dadswell HE, Wardrop AB. 1955. The structure and properties of tension wood. Holzforschung **9**, 97-104.

Decou R, Labrousse P, Béré E, Fleurat-Lessard P, Krausz P. 2020. Structural features in tension wood and distribution of wall polymers in the G-layer of in vitro grown poplars. Protoplasma **257**, 13-29.

Déjardin A, Leplé JC, Lesage-Descauses MC, Costa G, Pilate G. 2004. Expressed sequence tags from poplar wood tissues – a comparative analysis from multiple libraries. Plant Biology **6**, 55-64.

Derjaguin BV, Muller VM, Toporov, YP. 1975. Effect of contact deformations on the adhesion of particles. Journal of Colloid and Interface Science **53**, 314-326.

Eder M, Arnould O, Dunlop JWC, Hornatowska J, Salmén L. 2013. Experimental micromechanical characterisation of wood cell walls. Wood Science and Technology **47**, 163-182.

Fahlén J, Salmén L. 2002. On the lamellar structure of the tracheid cell wall. Pant Biology **4**, 339-345.

Fang CH, Clair B, Gril J, Alméras T. 2007. Transverse shrinkage in G-fibers as a function of cell wall layering and growth strain. Wood Science and Technology **41**, 659-671.

Fang CH, Clair B, Gril J, Liu S. 2008. Growth stresses are highly controlled by the amount of G-layer in poplar tension wood. IAWA Journal **29**, 237-246.

Fournier M, Alméras T, Clair B, Gril J. 2014. Biomechanical action and biological functions. In: Gardiner B, Barnett J, Saranpää P, Gril J, eds. The biology of reaction wood. Berlin: Springer, Berlin, 139-169.

Ghislain B, Nicolini EA, Romain R, Ruelle J, Yoshinaga A, Alford MH, Clair B. 2016. Multilayered structure of tension wood cell walls in *Salicaceae sensu lato* and its taxonomic significance. Botanical Journal of the Linnean Society **182**, 744-756.

Ghislain B, Clair B. 2017. Diversity in organisation and lignification of tension wood fibre walls – a review. IAWA Journal **38**, 245-265.

Ghislain B, Engel J, Clair B. 2019. Diversity of anatomical structure of tension wood among 242 tropical tree species. IAWA Journal **40**, 765-784.

Gindl W, Gupta HS, Grünwald C. 2002. Lignification of spruce tracheid secondary cell walls related to longitudinal hardness and modulus of elasticity using nano-indentation. Canadian Journal of Botany **80**, 1029-1033.

Gorshkova TA, Morvan C. 2006. Secondary cell-wall assembly in flax phloem fibres: role of galactans. Planta **223**, 149-158.

Gorshkova TA, Gurjanov OP, Mikshina PV, Ibragimova NN, Mokshina NE, Salnikov VV, Ageeva MV, Amenitskii SI, Chernova TE, Chemikosova SB. 2010. Specific type of secondary cell wall formed by plant fibers. Russian Journal of Plant Physiology **57**, 328-341.

Gorshkova TA, Mokshina N, Chernova T, Ibragimova N, Salnikov V, Mikshina P, Tryfona T, Banasiak A, Immerzeel P, Dupree P, Mellerowicz EJ. 2015. Aspen tension wood fibers contain β-(1→4)-galactans and acidic arabinogalactans retained by cellulose microfibrils in gelatinous walls. Plant Physiology **169**, 2048-2063.

783 **Gorshkova TA, Chernova T, Mokshina N, Ageeva M and Mikshina P.** 2018. Plant 'muscles':
784 fibers with a tertiary cell wall. New Phytologist **218**, 66-72.

785 **Goswami L, Dunlop JWC, Jungnikl K, Eder M, Gierlinger N, Coutand C, Jeronimidis G, Fratzl**
786 **P, Burgert I.** 2008. Stress generation in the tension wood of poplar is based on the lateral swelling
787 power of the G-layer. The Plant Journal **56**, 531-538.

788 **Goudenhooft C, Siniscalco D, Arnould O, Bourmaud A, Sire O, Gorshkova T, Baley C.** 2018.
789 Investigation of the mechanical properties of flax cell walls during plant development: the relation
790 between performance and cell wall structure. Fibers **6**, 6.

791 **Grozdits GA, Ifju G. 1969.** Development of tensile strength and related properties in differentiating
792 coniferous xylem. Wood Science **1**, 137-147.

793 **Guedes FTP, Laurans F, Quemener B, Assor C, Lainé-Prade V, Boizot N, Vigouroux J, Lesage-**
794 **Descauses MC, Leplé JC, Déjardin A, Pilate G.** 2017. Non-cellulosic polysaccharide distribution
795 during G-layer formation in poplar tension wood fibers: abundance of rhamnogalacturonan I and
796 arabinogalactan proteins but no evidence of xyloglucan. Planta **246**, 857-878.

797 **Huang Y, Fei B, Wei P, Zhao C.** 2016. Mechanical properties of bamboo fiber cell walls during the
798 culm development by nanoindentation. Industrial Crops and Products **92**, 102-108.

799 **Hermanowicz P, Sarna M, Burda K, Gabrys H.** 2014. AtomicJ: An open source software for
800 analysis of force curves. Review of Scientific Instruments **85**, 063703.

801 **Hock CW.** 1942. Microscopic structure of flax and related bast fibres. Journal of Research of the
802 National Bureau of Standards **29**, 41-50.

803 **Jäger A, Bader T, Hofstetter K, Eberhardsteiner J.** 2011. The relation between indentation
804 modulus, microfibril angle, and elastic properties of wood cell walls. Composites Part A: Applied
805 Science and Manufacturing **42**, 677-685.

806 **Jakes JE, Frihart CR, Beecher JF, Moon RJ, Stone DS.** 2008. Experimental method to account
807 for structural compliance in nanoindentation measurements. Journal of Materials Research **23**, 1113-
808 1127.

809 **Jakes JE, Frihart CR, Beecher JF, Moon RJ, Resto P, Melgarejo Z, Suárez OM, Baumgart H,**
810 **Elmustafa AA, Stone DS.** 2009. Nanoindentation near the edge. Journal of Materials Research **24**,
811 1016-1031.

812 **Johnson KL.** 1987. Contact mechanics. Cambridge University Press.

813 **Johnson KL, Greenwood JA.** 1997. An adhesion map for the contact of elastic spheres. Journal of
814 Colloid Interface Science **192**, 326-333.

815 **Konnerth J, Harper D, Lee SH, Rials TG, Gindl W**. 2008. Adhesive penetration of wood cell walls
816 investigated by scanning thermal microscopy (SThM). Holzforschung **62**, 91-98.

817 **Kozlova L, Petrova A, Ananchenko B, Gorshkova T.** 2019. Assessment of primary cell wall
818 nanomechanical properties in internal cells of non-fixed maize roots. Plants **8**, 172.

819 **Lafarguette F, Leplé JC, Déjardin A, Laurans F, Costa G, Lesage-Descauses MC, Pilate G.**
820 2004. Poplar genes encoding fasciclin-like Arabinogalactan proteins are highly expressed in tension
821 wood. The New Phytologist **164**, 107-121.

822 **Liang R, Zhu YH, Yang X, Gao JS, Zhang YL, Cai LP.** 2020. Study on the ultrastructure and
823 properties of gelatinous layer in poplar. Journal of Materials Science **56**, 415–427.

824 **Luo L, Zhu Y, JGui J, Yin T, Luo W, Liu J, Li L.** 2021. A comparative analysis of transcription
825 networks active in juvenile and mature wood in Populus. Frontiers in Plant Science **12**, 675075.

826 **Mellerowicz EJ, Gorshkova TA.** 2012. Tensional stress generation in gelatinous fibres: a review

and possible mechanism based on cell-wall structure and composition. Journal of Experimental Botany **63**, 551-565.

Meng Y, Xia Y, Young TM, Cai Z, Wang S. 2015. Viscoelasticity of wood cell walls with different moisture content as measured by nanoindentation. RSC Avances **5**, 47538.

Moulia B, Coutand C, Lenne C. 2006. Posture control and skeletal mechanical acclimation in terrestrial plants: implications for mechanical modeling of plant architecture. American Journal of Botany **93**, 1477-1489.

Nair SS, Wang S, Hurley DC. 2010. Nanoscale characterization of natural fibers and their composites using contact-resonance force microscopy. Composites: Part A **41**, 624-631.

Niklas KJ. 1992.Plant biomechanics. An engineering approach to plant form and function. Chicago: University of Chicago Press.

Normand AC, Charrier AM, Arnould O, Lereu AL. 2021. Influence of force volume indentation parameters and processing method in wood cell walls nanomechanical studies. Scientific Reports **11**, 5739.

Okumura S, Harada H, Saiki H. 1977. Thickness variation of the G-layer along a mature and a differentiating tension wood fiber in *Populus euramericana*. Wood Science and Technology **11**, 23-32.

Onaka F. 1949. Studies on compression and tension wood. Wood Research **1**, 1-88.

Özparpucu M, Rüggeberg M, Gierlinger N, Cesarino I, Vanholme R, Boerjan W, Burgert I. 2017. Unravelling the impact of lignin on cell wall mechanics: a comprehensive study on young poplar trees downregulated for CINNAMYL ALCOHOL DEHYDROGENASE (CAD). The Plant Journal **91**, 480-490.

Özparpucu M, Gierlinger N, Cesarino I, Burgert I, Boerjan W, Rüggeberg M. 2019. Significant influence of lignin on axial elastic modulus of poplar wood at low microfibril angles under wet conditions. Journal of Experimental Botany **70**, 4039-4047.

Peaucelle A. 2014. AFM-based mapping of the elastic properties of cell walls: at tissue, cellular, and subcellular resolutions. Journal of Visualized Experiments **89**, e51317.

Pérez-de-Lis G, Rathgeber CBK, Fernández-de-Uña L, Ponton S. 2022. Cutting tree rings into time slices: how intra-annual dynamics of wood formation help decipher the space-for-time conversion. New Phytologist **233**(3), 1520-1534.

Petrova A, Kozlova L, Gorshkov O, Nazipova A, Ageeva M, Gorshkova T. 2021. Cell wall layer induced in xylem fibers of flax upon gravistimulation is similar to constitutively formed cell walls of bast fibers. Frontiers in Plant Science **12**, 660375.

Pilate P, Déjardin A, Laurans F, Leplé JC. 2004. Tension wood as a model for functional genomics of wood formation. New Phytologist **164**, 63-72.

Pot G, Coutand C, Le Cam JB, Toussaint E. 2013a. Experimental study of the mechanical behaviour of thin slices of maturating green poplar wood using cyclic tensile tests. Wood Science and Technology **47**, 7-25.

Pot G, Toussaint E, Coutand C, Le Cam JB. 2013b. Experimental study of the viscoelastic properties of green poplar wood during maturation. Journal of Materials Science **48**, 6065-6073.

Pot G, Coutand C, Toussaint E, Le Cam JB, Saudreau M. 2014. A model to simulate the gravitropic response and internal stresses in trees, considering the progressive maturation of wood. Trees **28**, 1235-1248.

Richardson KC, Jarett L, Finke EH. 1960. Embedding in epoxy resins for ultrathin sectioning in electron microscopy. Stain Technology **35**, 313-323.

872 **Roach MJ, Deyholos MK.** 2007. Microarray analysis of flax (Linum usitatissimum L.) stems
873 identifies transcripts enriched in fibre-bearing phloem tissues. Molecular Genetics and Genomics
874 **278**, 149-165.

875 **Scurfield G.** 1973. Reaction wood: its structure and function. Science **179**, 647-655.

876 **Sell J, Zimmermann T.** 1998. The fine structure of the cell wall of hardwoods on transverse-fracture
877 surfaces. European Journal of Wood and Wood Products **56**, 365-366.

878 **Sudharshan Phani P, Oliver WC.** 2019. A critical assessment of the effect of indentation spacing
879 on the measurement of hardness and modulus using instrumented indentation testing. Materials and
880 Design **164**, 107563.

881 **Thibaut B, Gril J, Fournier M**. 2001. Mechanics of wood and trees: some new highlights for an old
882 story. Comptes Rendus de l'Académie des Sciences – Series IIB **329**, 701-716.

883 **Wagner L, Bader TK, De Borst K.** 2014. Nanoindentation of wood cell walls: effects of sample
884 preparation and indentation protocol. Journal of Materials Science **49**, 94-102.

885 **Wang X, Ren H, Zhang B, Fei B, Burgert I.** 2012. Cell wall structure and formation of maturing
886 fibres of moso bamboo (Phyllostachys pubescens) increase buckling resistance. Journal of the Royal
887 Society Interface **9**, 988-996.

888 **Xu D, Liechti KM, Ravi-Chandar K.** 2007. On the modified Tabor parameter for the JKR–DMT
889 transition in the presence of a liquid meniscus. Journal of Colloid and Interface Science **315**, 772-
890 785.

891 **Yoshinaga A, Kusumoto H, Laurans F, Pilate G, Takabe K.** 2012. Lignification in poplar tension
892 wood lignified cell wall layers. Tree Physiology **32**, 1129-1136.

893 **Zhang SY, Fei BH, Wang CG.** 2016. Effects of chemical extraction treatments on nano-scale
894 mechanical properties of the wood cell wall. BioResources **11**, 7365-7376.